JOURNAL OF MATERIALS SCIENCE 29 (1994) 6115–6122

R-curve behaviour of PZT ceramics near the morphotropic phase boundary

SUNGGI BAIK, SOO MIN LEE*
Department of Materials Science and Engineering, Pohang University of Science and Technology (POSTECH), Pohang 790-600, Korea

The mechanical failure of PZT ceramics was characterized by measuring *R*-curves for compositions near and at the morphotropic phase boundary (MPB) where tetragonal and rhombohedral phases coexist in equal quantities. The *R*-curve behaviours (an increasing fracture toughness with crack extension) were identified by indentation-fracture testing and they were analysed to determine the key parameters. The fracture toughness of the PZT ceramics consisted of three different terms, representing particular microstructural processes in front of advancing cracks, that is, intrinsic cleavage, 90° domain switching and microcracking. Their relative contributions to an overall crack-extension resistance varied with the length of the advancing crack and, more importantly, with the compositions of the PZT. In the compositional range where the tetragonal phase was dominant, the *R*-curves were determined by domain switching and microcracking. However, the compositional dependency of the fracture toughness was due to the microcracking mechanism. On the other hand, in regions rich in rhombohedral phases, the *R*-curves were essentially determined by domain switching in the crack-tip area. The *R*-curves characterized by the domain-switching mechanism were insensitive to the compositional variation near the MPB. Our results also demonstrated that *R*-curve analysis could be used to probe further into the microstructural responses of materials in front of advancing cracks and to quantify them particularly in systems like PZT where several different toughening processes compete with each other.

1. Introduction

The ferroelectric properties of polycrystalline PZT ceramics are highly sensitive to their compositions and microstructural characteristics [1, 2]. Specific applications require tailoring of their compositions, porosities, grain sizes, domain structures, etc. However, optimization of the ferroelectric properties does not necessarily guarantee the optimum mechanical stability of PZT ceramics. They often conflict with each other. The aim of this study is to establish the relationship between the mechanical failure of PZT ceramics and their compositions and microstructural variables by analysing *R*-curves near the morphotropic phase boundary (MPB), where the ferroelectric properties (such as the coupling coefficient and the relative permittivity) are usually maximized.

The solid solution system $Pb(Zr_xTi_{1-x})O_3$ exhibits a number of crystal structures which depend on x in the phase diagram of $PbZrO_3$–$PbTiO_3$ [3]. An abrupt structural change between tetragonal and rhombohedral phases occurs at the MPB, which is known to be close to $x = 0.535$ at room temperature for undoped PZT. Therefore, the MPB is a narrow region of x where tetragonal and rhombohedral phases coexist. It is a significant feature of the MPB that most of the ferroelectric properties change rapidly near the MPB and they often peak at the MPB. Hence, the compositions near the MPB have been heavily exploited in commercial applications. However, Freiman *et al.* [4] demonstrated that the critical fracture toughness, K_{IC}, of various commercial PZT components shows a distinct minimum at the MPB. The fracture- toughness data of Freiman *et al.* are reproduced in Fig. 1. A large decrease in K_{IC} is evident near the MPB. However, the data are insufficient (in number) to determine whether the minimum in K_{IC} is coincident with the exact position of the MPB. It has been already established that the MPB varies significantly and that it depends on the types and amounts of the dopants which are added in commercial compositions [3]. These dopants are not specified in the data presented in Fig. 1, which makes Fig. 1 unsatisfactory for use in the compositional formulation of PZT ceramics with the optimum mechanical stability.

Freiman *et al.* [4] argued that the minimum in the fracture toughness observed in PZT is due to a trade-off between the contributions from twinning (90° domain boundary motion) and from microcracking of grain-boundary facets with any residual tensile stress. Twinning is facilitated at the MPB, and it contributes

* *Present address*: Currently with the Samsung Advanced Institute of Technology, P.O. Box 111, Suwon, 440-600, Korea.

0022–2461

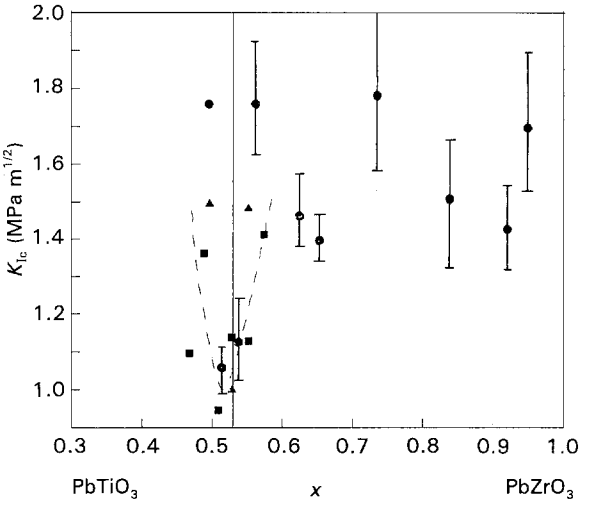

Figure 1 The fracture toughnesses of three different (●, ■, ▲) commercial PZT ceramics as a function of the compositions. The minimum in the fracture toughness appears near the MPB. (The data are reproduced from Freiman *et al.* [4]).

to the reduction of the crack-extension force. Away from the MPB, particularly towards the $PbTiO_3$ in the tetragonal phase field, the contribution of microcracking becomes increasingly important, while the twinning contribution diminishes. This explains the minimum in K_{IC}, because the toughening due to twinning is less effective than that due to microcracking. On the other hand, Mehta and Virkar [5] have convincingly demonstrated that domain switching (twinning) in the crack-tip stress field is a viable toughening mechanism in fully tetragonal PZT ceramics. The samples they used for fracture-toughness testing were commercial PZT ceramics with $x = 0.54$; the MPB of the composition should be located $x > 0.54$ because of the presence of unspecified dopants.

If any dilatational relaxation processes operate in front of or, on some occasions, behind the advancing crack (promoting an increase in the fracture toughness), *R*-curve behaviour would inevitably be observable [6]. The characteristics of *R*-curves (an increasing fracture toughness with crack extension) are sensitive to the micromechanics of the particular relaxation process at the crack-tip region. One of the most prominent examples can be found in partially stabilized zirconia (PSZ). Swain and Hannink [7] showed that a variety of microstructures could be produced by simply taking different thermal-processing routes using polycrystalline zirconia stabilized with 9.5 mol % MgO and that the characteristics of the *R*-curves which were determined afterwards were dramatically dependent on the microstructures. For PSZ containing tetragonal ZrO_2 precipitates which transform readily to monoclinic phases in a crack front, the *R*-curves quickly increased but saturated at high toughness values within 20–30 μm of the initial crack length. Whereas, for PSZ with a continuous m-ZrO_2 phase showing extensive microcracking and crack branching, the *R*-curves increased slowly but continuously over a large crack extension up to a few hundred micrometres. Furthermore, in the case of polycrystalline alumina, the *R*-curves continuously increased up to crack lengths of a few millimetres; this behaviour is believed to originate from the bridging of unbroken ligaments of the grains in the crack wake [8].

Evidence of the *R*-curve behaviour in ferroelectric materials was, in fact, presented by Okazaki in 1984 [9]. However, as pointed out in 1990 by Mehta and Virkar [5], Okazaki's interpretation of the observed dependency of the fracture toughness on the indentation-crack sizes was incorrect. The parabolic dependency of K_{IC} on the crack length, c, is not due to residual stress, but is probably due to an *R*-curve behaviour. A non-linear dependence of the logarithm fracture strength of the logarithm of the indentation load in PZT with $x = 0.95$ was also mistakenly interpreted in terms of the residual stress in [4]. Pohanka and co-workers [10, 11] uncovered a strong correlation between K_{IC} and the microstructural parameters (for example the grain size) in another commercially-important ferroelectric material, that is, $BaTiO_3$. Cook *et al.* [12] subsequently reinterpreted this correlation in terms of an *R*-curve behaviour.

The special features that are found on examination of the *R*-curves of polycrystalline ceramics include the following features. Firstly, the dimensionality of the microstructural parameters which affect the crack-tip stress field can be identified because the critical crack size below which a rising K_{IC} can be observed is believed to be directly related to the size of the toughening zone in front of the crack tip. Secondly, it provides us with asymtotic values of K_{IC} at the higher end of the crack-size spectrum, which can be safely used for the evaluation of the effectiveness of particular compositional or microstructural variations in the fracture resistance. In this study, we characterized the *R*-curves for PZT ceramics as a function of compositions within a narrow compositional range which included the MPB.

2. Experimental procedures

The compositions selected for the present study were: (i) $Pb_{0.94}Sr_{0.06}(Zr_xTi_{1-x})O_3$, a typical hard PZT, with x varying between 0.50 and 0.60; and (ii) $Pb(Mg_{1/3}Nb_{2/3})_{0.25}(Zr_xTi_{1-x})_{0.75}O_3$, a typical PMN–PZT ceramic, with x between 0.38 and 0.54. The selection of the x-values in these two cases was based on the phase diagrams of $PbZrO_3$–$PbTiO_3$ [3] and of $Pb(Mg_{1/3}Nb_{2/3})O_3$–$PbZrO_3$–$PbTiO_3$ [13], respectively, so that the MPB could be placed safely within the chosen compositional ranges. The procedures for the sample preparation have been reported elsewhere [14]. For PMN–PZT samples, magnesium niobate ($MgNb_2O_5$) powder was prepared first according to procedures proposed by Schwartz and Shrout [15] in order to prevent pyrochlore phase formation. Subsequent processing followed the procedures described in [14]. About 3.0 mol % of excess PbO was added to all the compositions in order to compensate for PbO loss during calcination and sintering. Moreover, in order to minimize PbO loss during sintering, a PbO-rich atmosphere was maintained by placing environmental powder ($PbZrO_3$

+ 10wt % ZrO_2) within a closed alumina crucible [16]. Final densities were determined by the Archimedes technique following the relevant ASTM standard [17]; and the grain sizes were measured by the linear intercept method.

The crystalline phases, and their lattice constants, were determined by X-ray diffraction (XRD) of the powdered samples made from the sintered pellets. The relative amount of each of the tetragonal (T) and rhombohedral (R) phases, was determined by measuring the integrated intensities of the corresponding XRD peaks, T(2 0 0) + T(0 0 2) and R(2 0 0), respectively. These overlapping peaks were separated using a multiple-peak separation program (Rigaku, Japan) before the integration. The percentage of each phase was calculated using the following equation. For instance, for the *R*-phase,

$$R - \text{phase percentage} = \frac{I_{R(2\,0\,0)}}{I_{T(2\,0\,0)} + I_{T(0\,0\,2)} + I_{R(2\,0\,0)}} 100$$

where the I represents the integrated intensities of the corresponding XRD peaks. The difference in their structural factors was assumed to be negligible. The lattice constants were determined by using a lattice-constant refinement program (Rigaku, Japan).

Some of the samples were selected for Vickers indentation and subsequent uniaxial four-point-bending tests. The dimensions of the bending bars were $3 \times 4 \times 25\ mm^3$. After machining, they were polished and annealed at 1100 °C for 30 min to eliminate surface flaws and residual stresses prior to the testing. The edges of the specimens were rounded. Some of the specimens were electrically poled in the direction parallel or perpendicular to the crack-advancing plane [5, 9, 18]. An electric field of 2.5 kV mm^{-1} was applied for 3 min at 100 °C in a dielectric oil. The specimens were indented at the centre of their tensile faces with a Vickers diamond pyramid. The indentation loads were varied from 5 to 200 N. All the indentations were made in air with a steady loading rate that required 15 s to produce a full load and the full load was applied for another 10 s. Care was taken to orient one set of radial cracks in a normal direction to the tensile axis. A drop of silicon oil was placed at the indentation site immediately after the indentation to minimize fatigue effects [18]. Uniaxial bending tests were performed in a four-point-bending fixture with a 7 mm inner span and a 23.5 mm outer span. The bending strength was calculated from the following equation:

$$S = \frac{3F(l_1 - l_2)}{2bt^2} \quad (1)$$

where F was the maximum load required to break the specimen, $l_1 = 23.5$ mm, $l_2 = 7$ mm, $b = 4$ mm and $t = 3$ mm. The strength data were taken only from samples which failed at the indentation sites.

3. Results

Table 1 summarizes the phases identified, the densities and the grain sizes of the PZT and the PMN–PZT ceramics prepared for mechanical testing. The variations in the final densities and in the grain sizes are insignificant in comparison to the phase change observed. The fractional amount of each phase within the MPB region where the T- and R-phases coexist was determined from the XRD patterns illustrated in Fig. 2, after separating the overlapping T(2 0 0), T(0 0 2) and R(2 0 0) peaks, as demonstrated in Fig. 3. The MPB regions where the two phases are coexistent were in the composition range $x = 0.51$–0.57 for the SrO-doped PZT (Sr–PZT), and in the range $x = 0.40$–0.50 for the PMN–PZT ceramics. As shown in Fig. 4, the exact MPB where the two phases are in equal quantities appeared at $x = 0.554$ for Sr–PZT and at $x = 0.46$ for PMN–PZT. Apparently, the doping of 0.06 mol % SrO induced a significant shifting of the MPB towards the R-phase field, while the doping of 25 mol % of PMN in the PZT shifted the MPB

TABLE I Microstructural characteristics of the Sr–PZT ($Pb_{0.94}Sr_{0.06}(Zr_xTi_{1-x})O_3$) and the PMN–PZT ($Pb(Mg_{1/3}Nb_{2/3})_{0.25}(Zr_xTi_{1-x})_{0.75}O_3$) ceramics prepared for the mechanical testing

Specimen	x	Phases[b]	Density ($kg\ m^{-2}$)	Grain size (μm)
Sr–PZT50	0.50	T	74.0	6.5
Sr–PZT51[a]	0.51	T	73.6	5.6
Sr–PZT52	0.52	T + R	74.5	6.0
Sr–PZT53	0.53	T + R	74.5	6.3
Sr–PZT54[a]	0.54	T + R	74.8	8.0
Sr–PZT55[a]	0.55	T + R	76.2	6.0
Sr–PZT57	0.57	R	75.2	7.1
Sr–PZT60[a]	0.60	R	76.3	10.9
PMN–PZT38[a]	0.38	T	74.8	3.8
PMN–PZT40	0.40	T + R	75.0	3.3
PMN–PZT42	0.42	T + R	75.5	3.6
PMN–PZT44	0.44	T + R	75.1	3.2
PMN–PZT46[a]	0.46	T + R	76.0	3.9
PMN–PZT48	0.48	T + R	77.6	5.1
PMN–PZT50	0.50	T + R	78.0	4.2
PMN–PZT52	0.52	R	76.1	3.7
PMN–PZT54[a]	0.54	R	76.8	4.8

[a] Specimens for indentation–strength measurements.
[b] R = rhombohedral phases and T = tetragonal phases.

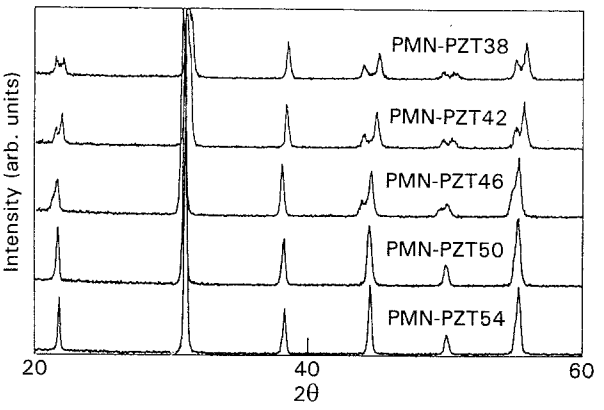

Figure 2 XRD data for the PMN–PZT ceramics, showing the phase changes from the tetragonal phase to the rhombohedral phase as the composition changed from $x = 0.38$ to 0.54.

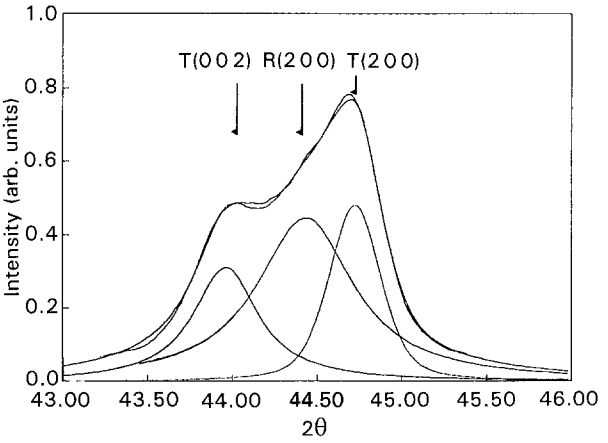

Figure 3 The fractional amounts of the tetragonal and the rhombohedral phases determined by integrating the separated {200} XRD peaks.

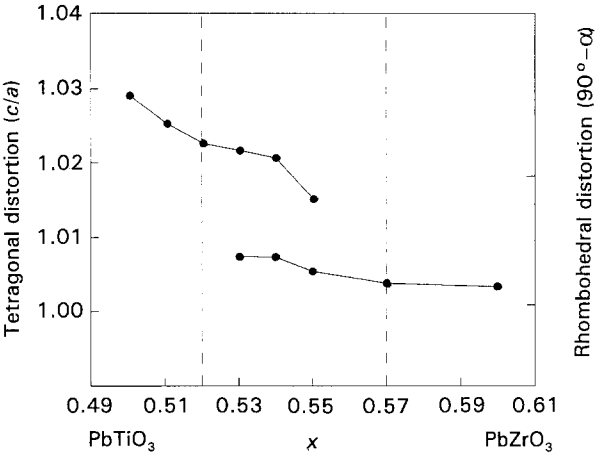

Figure 5 Unit-cell distortions at room temperature for tetragonal (upper curve) and rhombohedral (lower curve) phases for Sr–PZT ceramics near the MPB.

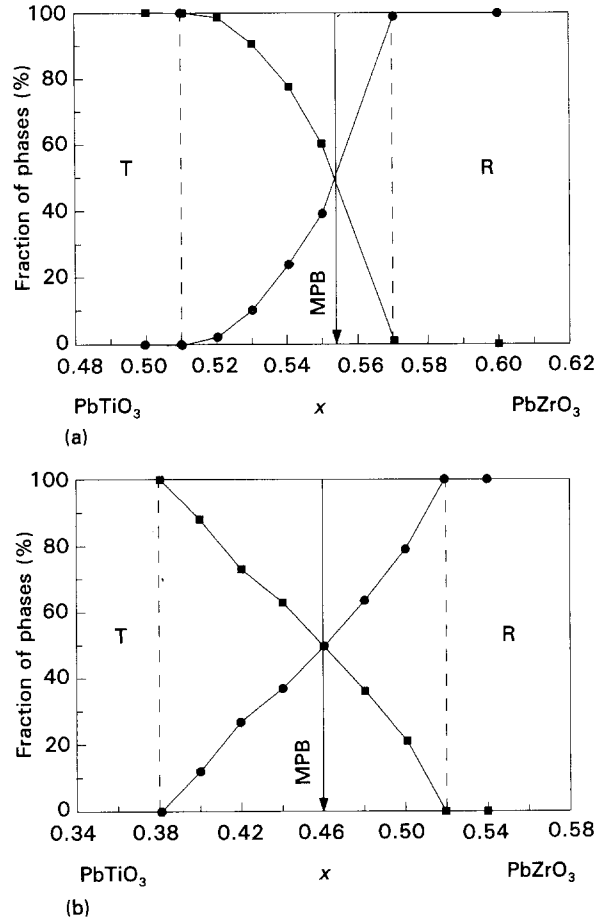

Figure 4 The percentage fraction of the tetragonal and the rhombohedral phase near the MPB for: (a) Sr–PZT, and (b) PMN–PZT.

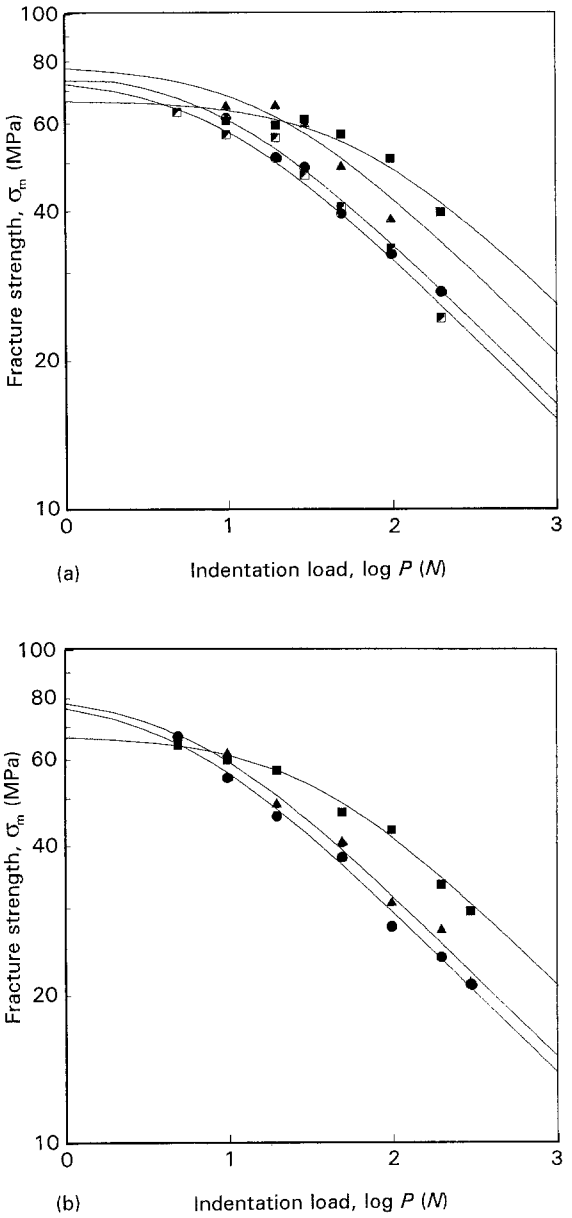

Figure 6 Plots of the fracture strength as a function of the indentation load for: (a) the Sr–PZT ceramics, (■) Sr–PZT51, (▲) Sr–PZT54, (◩) SR–PZT55, and (●) Sr–PZT60; and (b) the PMN–PZT ceramics (■) PMN–PZT38, (▲) PMN–PZT54, and (●) PMN–PZT46.

towards the T-phase field significantly. It is also interesting to note that, contrary to the suggestion by Nomura and co-workers [19], a simple lever rule cannot be applied to determine the phase quantity within the MPB region, particularly for Sr–PZT ceramics. Unit-cell distortions of the T-phase (c/a) and the R-phase (90°-α) were determined, and they are plotted in Fig. 5.

Fig. 6 a is plot of the fracture strength, σ_m, versus the indentation load, P, for some of the samples in

Table I. The data were only taken from samples which failed at an indentation site. A distinctive feature of the data is that all the curves approach a plateau at lower values of the indentation load. This is a definitive demonstration of R-curve behaviour [12]. Interestingly, the asymptotic values of σ_m for the lower values of P are almost identical. This indicates that the flexural strength of the material does not change greatly when its composition and phases vary. On the other hand, the critical indentation load, P^*, below which R-curve behaviours are observable changes significantly as the composition moves away from MPB toward the T-phase field. At the higher limit of P, $\log \sigma_m$ becomes linearly dependent on $\log P$, with a slope of $-1/3$. This suggests that $\sigma_m P^{1/3}$ is asymptotically approaching a constant value and that the asympotic values of the fracture toughness which are independent of P (or c), can be obtained from linear indentation fracture mechanics [20] according to the analysis in the next section.

4. *R*-curve analysis

Cook *et al.* [12] proposed a closed-form solution of an apparent fracture toughness as a function of the indentation load from a simple extension of the indentation–fracture mechanics [20]. This solution has also been shown to be reasonably applicable to analysis of the indentation–fracture testing results of various ceramic materials, including $BaTiO_3$. The proposed equation of the fracture strength as a function of the indentation load is

$$\sigma_m = \sigma_f[P^*/(P + P^*)]^{1/3} \quad (2)$$

where σ_f denotes the asymptotic value of σ_m in the limit of small cracks. Then, the critical fracture toughness over the entire range of P can be obtained from an equation given by Chantikul *et al.* in [20]; that is,

$$K_c = 0.88\,(\sigma_m P^{1/3})^{3/4} \quad (3)$$

It is thus possible to define the R-curve function $K_c(P)$ by combining Equations 2 and 3 so that

$$K_c = K_c^\infty[P/(P + P^*)]^{1/4} \quad (4)$$

where K_c^∞ represents the upper limit of the toughness in the high-P region. Hence, the value of K_c^∞ may be calculated directly from

$$K_c^\infty = 0.88\,\sigma_f^{3/4}\,(P^*)^{1/4} \quad (5)$$

using values of σ_f and P^* determined from Equation 2. The solid lines in Fig. 6 represent least-squares fits (using Equation 2) to the experimental data with two adjusting parameters, σ_f and P^*. The fitting is surprisingly good. The resulting R-curves computed using Equation 4 are shown in Fig. 7. The cut-off values for K_c at the low-P end of the curves were adopted as 0.6 MPa $m^{1/2}$ for Sr–PZT and 0.5 MPa $m^{1/2}$ for PMN–PZT. These values were determined from specimens which were electrically poled perpendicular to the crack plane (see the discussion in Section 5). If K_0 represents an intrinsic cleavage-fracture toughness which is insensitive to x or P, then K_c can be defined

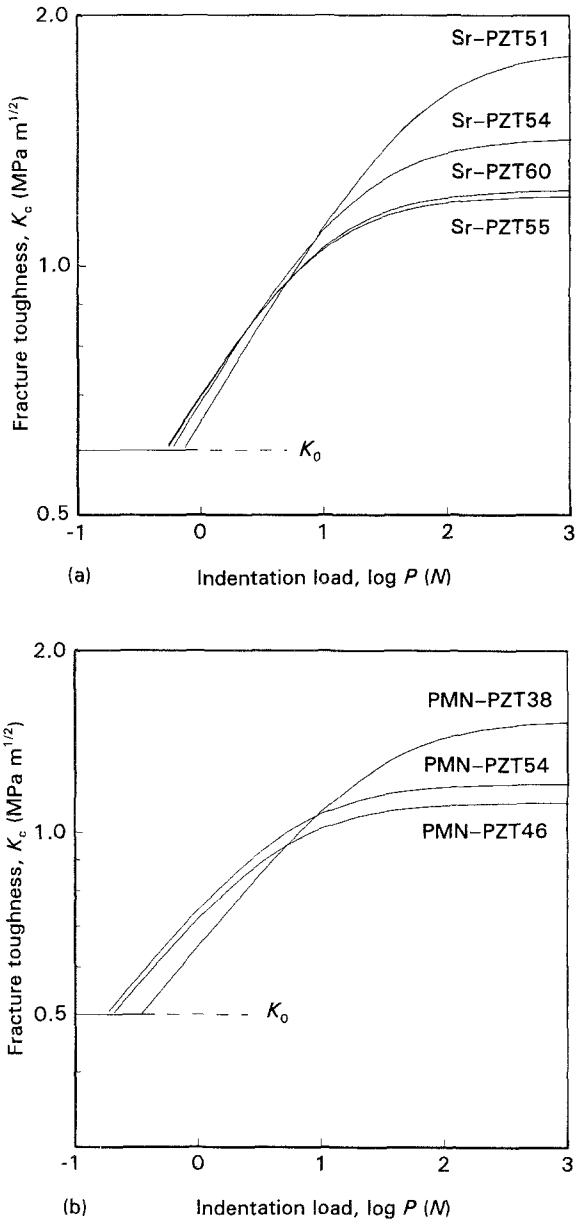

Figure 7 R-curves determined by the indentation–fracture testing and presented as a function of the indentation load for: (a) Sr–PZT, and (b) PMN–PZT.

as

$$K_c(P) = K_0 + K_\mu(P) \quad (6)$$

where $K_\mu(P)$ denotes all the microstructural contributions to the fracture toughness. Now, the remaining task is to define $K_\mu(P)$ in terms of the microstructural parameters of the relevant toughening processes.

Table II summarizes the values of key parameters which were determined. For each P^*, a critical crack length, c^*, can also be estimated; and this might be correlated to a zone size for the relevant toughening process. Estimated values of c^*, and their normalized values with respect to average grain sizes, are also included in Table II.

5. Discussion

It has been shown that the indentation–strength test data could be reasonably described by the R-curve model proposed by Cook *et al.* [12]. The major

TABLE II Indentation–fracture parameters of PZT ceramics

Composition	σ_f(MPa)	P^*(N)	K_c^{∞}(MPa m$^{1/2}$)	c^*(μm)	c^*/d)
Sr–PZT51	67	61	1.82	203	36
Sr–PZT54	77	16	1.43	97	12
Sr–PZT55	75	8	1.21	69	12
Sr–PZT60	76	9	1.24	73	7
PMN–PZT38	67	31	1.54	129	39
PMN–PZT46	81	5	1.13	47	12
PMN–PZT54	84	6	1.21	51	11

criticism of this model was that it has often been impossible to obtain a in slope of $-1/3$ at large indentation loads in the plot of log σ_m against log P, particularly in large-grained alumina [21] and whisker-toughened ceramic composites [22]. However, alternative power-law descriptions do not adequately fit all the data over a wide indentation-load spectrum for a single value of the power-law exponent. A justification for adopting the model proposed by Cook *et al.* [12] for PZT ceramics lies in the fact that typically the dimension of the toughening zone influencing increasing values of K_μ is limited to within about 30 grains (at most) in front of the crack tip (see Table II).

As discussed in Section 1, microcracking and twinning (domain switching) have been identified as the dominant toughening mechanisms in PZT ceramics near the MPB [4, 5, 10, 11]. The relative contributions of each process to the toughness should vary as the composition or as the microstructure changes. However, the contributions to the crack-tip stress relaxation are additive, and thus

$$K_\mu(P) = K_M(P) + K_D(P) \quad (7)$$

where K_M represents the toughness due to microcracking and K_D is the toughness due to domain switching. Combining Equations 6 and 7 gives

$$K_c(P) = K_0 + K_M(P) + K_D(P). \quad (8)$$

In order to interpret the R-curves shown in Fig. 7, it is necessary to separate each term in Equation 8 for a given composition. Our approach was to measure the fracture toughnesses of each of the samples which were electrically polarized in the direction perpendicular to the crack plane. By first electrically orienting the 90°-domains in the direction of the tensile axis in front of the crack tip it was possible to eliminate a potential contribution to the domain switching [5, 23]. Fig. 8 compares the toughness values determined by the indentation technique for the poled and unpoled samples as a function of the compositions. The toughness decreased monotonically as the composition approached the MPB from the T-phase field. It reached a minimum at the MPB, and it remained almost constant as the fraction of the R-phase increased. The difference between the two phases represents the asymptotic value of toughness due to domain switching, K_D. It is interesting to note that $K_D(P)$ is essentially independent of the compositional change near the MPB. Now, assume that the contribution from the microcracking, K_M, in the R-phase field is

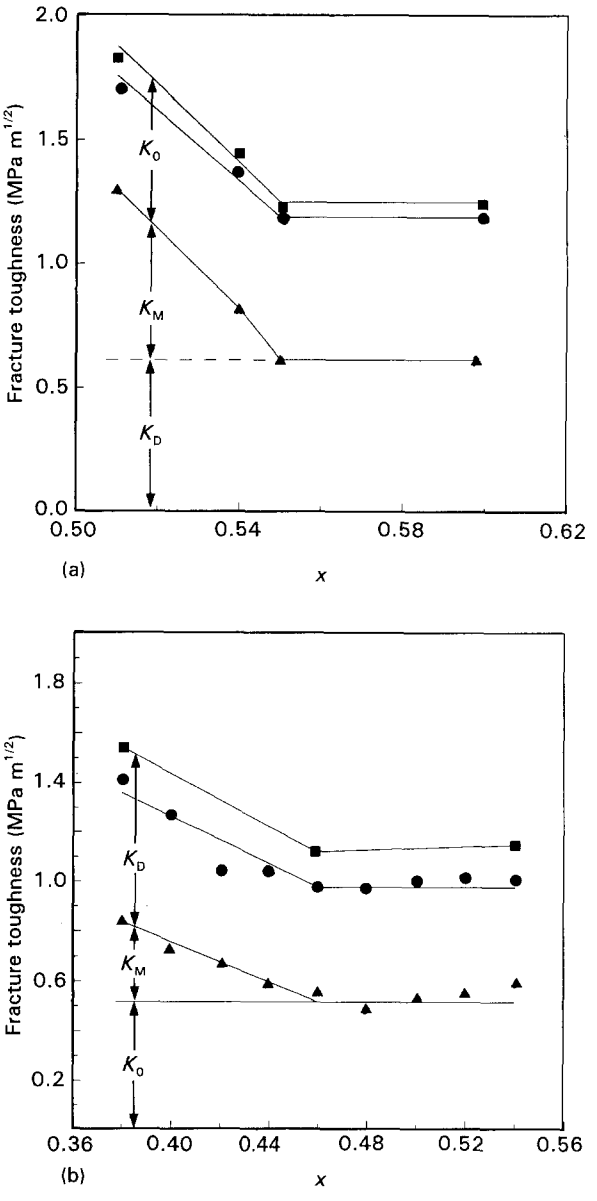

Figure 8 The asymptotic values of the fracture toughness which consists of three different terms; the intrinsic cleavage K_0, the toughness due to domain switching, K_D, and the microcracking, K_M. for: (a) Sr–PZT, and (b) PMN–PZT. (■) K_C^{∞} (IF method), (●) K_C (indentation), and (▲) K_C (poled). The compositional dependency is mainly due to the microcracking contribution.

negligible due to the fact that the residual stresses produced by a rhombohedral distortion are much smaller than those produced by a tetragonal distortion (see Fig. 5). Then the constant values of the toughness determined by an indentation test using the samples poled perpendicular to the crack planes can

be adopted as K_0, the intrinsic cleavage fracture toughness, which is also independent of the compositional change near the MPB. Hence, it becomes clear that the major component of the fracture toughness which is dependent on the compositional changes near the MPB is the contribution due to microcracking, $K_M(P)$. As shown in Fig. 8, $K_M(P)$ can be determined by substracting K_0 and K_D from K_c. The increase in the fracture toughness as the compositions move from the MPB towards the T-phase field is due to the fact that K_M depends strongly on the compositions of the PZT ceramics.

Hutchinson [24] analysed the microcracking behaviour in brittle materials and showed that $K_M \sim E\theta h^{1/2}$, where E is the modulus, θ is the misfit strain caused by microcracks and h is the microcracking zone size under a steady-state-crack-growth condition. Supposing that h scales with c^*, then

$$K_M = B\varphi_T(c/a - 1)(c^*)^{1/2} \quad (9)$$

where B is a proportionality constant, and φ_T is the fraction of the T-phase which is present. Using the data in Fig. 4, and Fig. 5, and Table II, K_M was plotted in Fig. 9 for the compositions within the T-phase field. More data are needed to test the validity of Equation 9 properly. However, the linearity between K_M and $\varphi_T(c/a - 1)(c^*)^{1/2}$ is quite good. From the slope of the line shown in Fig. 9, the estimated value of B is 2.86 GPa.

The implication of our analysis on the R-curve characteristics of PZT ceramics near the MPB is summarized schematically in Fig. 10. The R-curve of K_D rises faster than that of K_M in the small-crack region. This implies that, in the limit of small cracks where the crack extension behaviour of natural flaws can be assimilated, the twinning at the crack front is the dominant mechanism in the resistance to crack extension; whereas, the microcracking will play an increasingly important role as the crack grows. However, the microcracking contribution to the fracture toughness is significant only in the T-phase field.

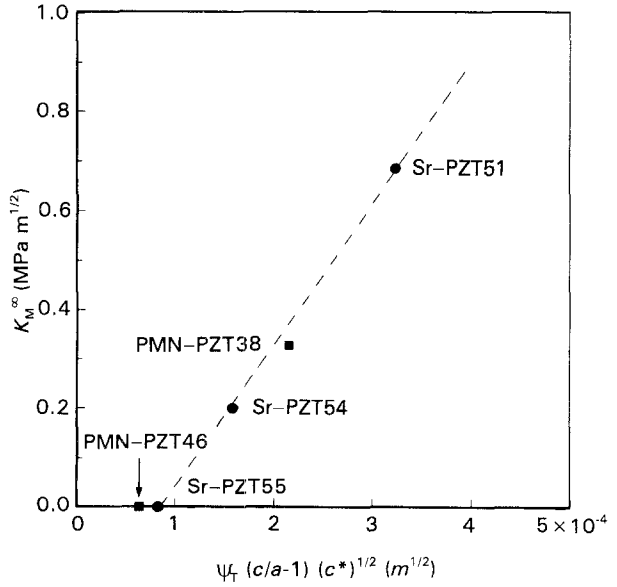

Figure 9 The microcracking contribution to the toughness plotted as a function of the parameter defined in Equation 9. B is estimated from the slope of the dashed line.

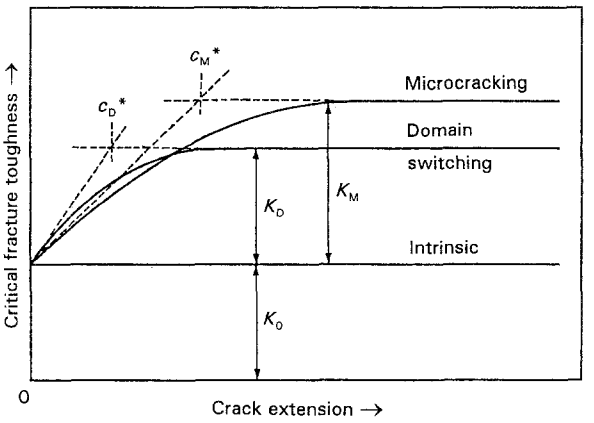

Figure 10 Schematic R-curves observed in PZT ceramics near the MPB.

The effects of the microstructural characteristics on the fracture toughness of PZT ceramics can be reassessed on the basis of our analysis. For instance, the change in the grain size would affect each term in Equation 8 differently. Firstly, K_0 should not be influenced by the grain size as long as the change in the grain size does not induce the change in the mode of fracture from intergranular to transgranular, or vice versa. Secondly, K_D would be insensitive to the grain size as long as the grain size is greater than the domain size. The dilatational strain caused by 90° domain switching is proportional to the size of twins, which is believed to be essentially constant above a critical grain size; for instance, this is about 10 μm in the case of $BaTiO_3$ [25]. No attempt has been made to quantify the critical grain size in PZT ceramics. Recent TEM studies [26] of undoped PZT with MPB compositions showed that the average width of the 90° domains was of the order of 0.1 μm. It is thus expected that the average twin size is invariant as long as the grain size is in the order of a few micrometers. However, in fine-grained PZT ceramics, the domain structure would be affected by the grain size, and K_D would be influenced by the variation in the grain size. Finally, K_M will certainly be the term that should be affected by the change in the grain size. The increase in K_c with increasing grain size has been observed in $BaTiO_3$ [10]. According to Equation 9, it is consistent with our model. The size and population of the mirocracks should influence c^*, the critical crack size, which is related to the microcracking zone size.

The results shown in Fig. 8 are inconsistent with the results of Freiman *et al.* [4, 10] that are shown in Fig. 1, particularly in the R-phase field. Freiman *et al.* reported that the toughness increased from the minimum at the MPB as the composition shifted toward R-phase field. A stress-induced phase transformation from the R-phase to the T-phase was suggested as a possible cause of this increase. We could not observe such an increase in the R-phase field. This discrepancy might originate from the difference in the nominal compositions employed in the experiment, and further study is necessary for clarification. A quantitative XRD study on fracture planes of the specimens rich in R-phases may help resolve the issue.

6. Conclusions

Indentation–fracture testing for 6 mol % SrO-doped PZT ceramics, $Pb_{0.94}Sr_{0.06}(Zr_xTi_{1-x})O_3$, and 25 mol % PMN-doped PZT ceramics, $Pb(Mg_{1/3}Nb_{2/3})_{0.25}(Zr_xTi_{1-x})_{0.75}O_3$, was used to investigate the *R*-curve behaviours as a function of x near the MTB. The most important findings from this investigation are as follows.

1. The MPBs in which both rhombohedral and tetragonal phases coexist were in the range, $x = 0.51$–0.57 for Sr–PZT and $x = 0.40$–0.50 for PMN–PZT, and the exact MPBs where they exist in equal fractions were at $x = 0.554$ for Sr–PZT and at $x = 0.46$ for PMN–PZT.

2. Strong *R*-curve behaviours were observed with different critical indentation loads (or crack lengths) depending on the composition, x; this suggests that the toughening mechanism varies with the compositions near the MPB.

3. The analysis of the *R*-curves supplemented with the indentation toughness results of electrically poled specimens showed that 90° domain switching (twinning) was primarily responsible for the *R*-curve behaviour in the compositional region rich in the *R*-phase, but it was insensitive to the compositional variation within the region.

4. On the other hand, both microcracking and twinning caused *R*-curve behaviours in the region rich in T-phases. In particular, the toughness due to microcracking was strongly dependent on the compositional variation near the MPB.

5. The asymptotic values of the toughness for larger indentation loads (or crack lengths) were a minimum at the MPB, as previously reported. However, in contrast to the results in 4, these values remained constant at the minimum as the composition moved away from the MPB toward the R-phase field.

Acknowledgements

The authors thank the Korean Ministry of Commerce and Industry for financial assistance, and G. M. Choi and S. T. Jun for helpful discussions throughout this study.

References

1. J. M. HERBERT, in "Ferroelectric transducers and sensors" (Gordon and Breach, New York, 1982).
2. A. J. MOULSON and J. M. HERBERT, in "Electroceramics" (Chapman and Hall, London, 1990).
3. B. JAFFE, W. R. COOK and H. JAFFE, in "Piezoelectric ceramics" (Academic Press, London, 1971).
4. S. W. FREIMAN, L. CHUCK, J. J. MECHOLSKY, D. L. SHELLEMAN and L. J. STORZ, in "Fracture mechanics of ceramics", Vol. 8, edited by R. C. Bradt, A. G. Evans, D. P. H. Hasselman and F. F. Lange (Plenum Press, New York, 1986) p. 175.
5. K. MEHTA and A. V. VIRKAR, *J. Amer. Ceram. Soc.* **73** (1990) 567.
6. A. G. EVANS, *ibid.* **73** (1990) 187.
7. M. V. SWAIN and R. H. J. HANNINK, in "Advances in ceramics", Vol. 12, edited by N. Claussen, M. Ruhle and A. H. Heuer (American Ceramic Society, Columbus, OH, 1984).
8. R. W. STEINBRECH, A. REICHL and W. SCHAARWACHTER, *J. Amer. Ceram. Soc.* **73** (1990) 2009.
9. K. OKAZAKI, *Amer. Ceram. Soc. Bull.* **63** (1984) 1150.
10. R. C. POHANKA, S. W. FREIMAN, K. OKAZAKI and S. TASHIRO, in "Fracture mechanics of ceramics", Vol. 5, edited by R. C. Bradt, A. G. Evans, D. P. H. Hasselman and F. F. Lange (Plenum Press, New York. 1983) p. 356.
11. R. C. POHANKA, P. L. SMITH and S. W. FREIMAN, in "Electronic ceramics", edited by L. M. Levinson (Marcel Dekker, New York, 1988) p. 51.
12. R. F. COOK, B. R. LAWN and C. J. FAIRBANKS, *J. Amer. Ceram. Soc.* **68** (1985) 604.
13. H. OUCHI, K. NAGANO and S. HAYAKAWA, *ibid.* **48** (1965) 630.
14. S. BAIK, S. M. LEE and B. S. MIN, in "Fracture mechanics of ceramics", Vol. 9, edited by R. C. Bradt, D. P. H. Hasselman, D. Munz, M. Sakai and V. Ya. Shevchenko (Plenum, New York, 1992).
15. S. L. SHWARTZ and T. R. SHROUT, *Mater. Res. Bull.* **17** (1982) 1245.
16. A. I. KINGON and J. B. CLARK, *J. Amer. Ceram. Soc.* **66** (1983) 253.
17. ASTM Standard C20-46 (American Society of Testing and Materials, Philadelphia, 1969).
18. J. C. BRUCE, W. W. GERBERICH and B. G. KOEPKE, in "Fracture mechanics of ceramics", Vol. 4, edited by R. C. Bradt, A. G. Evans, D. P. H. Hasselman and F. F. Lange (Plenum Press, New York, 1978).
19. L. HANH, K, UCHINO and S. NOMURA, *Jpn. J. Appl. Phys.* **17** (1978) 637.
20. P. CHANTIKUL, G. R. ANSTIS and B. R. LAWN, *J. Amer. Ceram. Soc.* **64** (1981) 539.
21. R. F. KRAUSE, *ibid.* **71** (1988) 338.
22. J. HOMENY and W. L. VAUGHN, *ibid.* **73** (1990) 2060.
23. G. G. PISARENKO, V. M. CHUSHKO and S. P. KOVALEV, *ibid.* **68** (1985) 259.
24. J. W. HUTCHINSON, *Acta Metall.* **35** (1987) 1605.
25. G. ARLT and P. SASKO, *J. Appl. Phys.* **51** (1980) 4956.
26. P. G. LUKUTA, *J. Amer. Ceram. Soc.* **72** (1989) 933.

Received 2 February
and accepted 27 May 1994